THE JOURNAL OF PHYSICAL CHEMISTRY B

Article

pubs.acs.org/JPCB

The Role of Molecular Conformation and Polarizable Embedding for One- and Two-Photon Absorption of Disperse Orange 3 in Solution

Daniel L. Silva,*[,†] N. Arul Murugan,[‡] Jacob Kongsted,[§] Zilvinas Rinkevicius,[‡] Sylvio Canuto,[†] and Hans Ågren[‡]

[†]Instituto de Física, Universidade de São Paulo, Caixa Postal 66318, 05314-970 São Paulo, SP, Brazil

[‡]Department of Theoretical Chemistry and Biology, School of Biotechnology, Royal Institute of Technology, SE-106 91 Stockholm, Sweden

[§]Department of Physics, Chemistry and Pharmacy, University of Southern Denmark, Campusvej 55, DK-5230 Odense M, Denmark

ABSTRACT: Solvent effects on the one- and two-photon absorption (1PA and 2PA) of disperse orange 3 (DO3) in dimethyl sulfoxide (DMSO) are studied using a discrete polarizable embedding (PE) response theory. The scheme comprises a quantum region containing the chromophore and an atomically granulated classical region for the solvent accounting for full interactions within and between the two regions. Either classical molecular dynamics (MD) or hybrid Car−Parrinello (CP) quantum/classical (QM/MM) molecular dynamics simulations are employed to describe the solvation of DO3 in DMSO, allowing for an analysis of the effect of the intermolecular short-range repulsion, long-range attraction, and electrostatic interactions on the conformational changes of the chromophore and also the effect of the solute−solvent polarization. PE linear response calculations are performed to verify the character, solvatochromic shift, and overlap of the two lowest energy transitions responsible for the linear absorption spectrum of DO3 in DMSO in the visible spectral region. Results of the PE linear and quadratic response calculations, performed using uncorrelated solute−solvent configurations sampled from either the classical or hybrid CP QM/MM MD simulations, are used to estimate the width of the line shape function of the two electronic lowest energy excited states, which allow a prediction of the 2PA cross-sections without the use of empirical parameters. Appropriate exchange-correlation functionals have been employed in order to describe the charge-transfer process following the electronic transitions of the chromophore in solution.

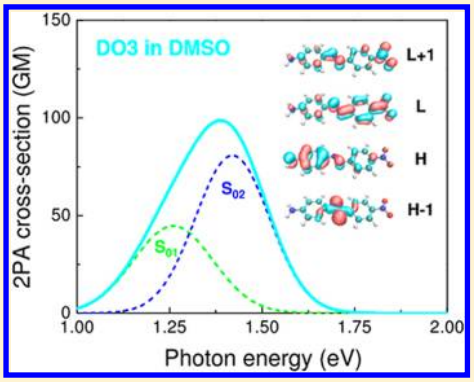

1. INTRODUCTION

Azocompounds cover a wide variety of molecules showing particular spectral features that can be traced to the presence of the azo group (−N═N−).[1−3] Among the azocompounds, the azoaromatic molecules, with two aromatic rings linked by the azo group, are probably the most widely studied. The addition of donor and acceptor groups at the ends of the aromatic rings introduces low-lying charge-transfer excited states and shifts the absorption and emission bands to the visible (vis) spectral region,[1,2] something that is strongly dependent on the interaction with a solvent.[4−7]

A large number of studies on the electronic and optical properties of the azoaromatic molecules have been conducted throughout the years and presented in the literature.[3,8] Of particular interest is the influence of the molecular structure of these molecules on their one-photon and two-photon absorption (1PA and 2PA, respectively) processes,[9−13] for example, the effect of conjugation length,[10] the molecular symmetry, and the presence and strength of donor and acceptor groups on the absorption.[9,11−13] In addition, experimental and theoretical studies have also been carried out for understanding how a solvent can affect the 1PA and 2PA processes.[14−16] While extensive efforts have long been devoted to obtain structure−property relationships to better explore or improve the 1PA and 2PA absorption,[9,17−21] the effect of molecular conformation on the processes has attracted interest in more recent times.[22−25] In the experimental context, several studies have shown that the conformation of the azoaromatic molecules can be altered, for example, by a change of temperature in such a way that a dynamic control of the absorption processes can be performed.[22,24] In the first theoretical studies, the molecular conformation was manually changed by altering the main torsional/dihedral angles of the molecules for a posteriori quantum mechanical calculations.[13,26,27] Later, classical molecular dynamics (MD) simulations emerged as an effective way to describe molecular conformations of the solute in a solvent environment adopting a well-defined thermodynamic condition and to investigate the effect of the conformational changes on its 1PA and 2PA processes.[23,25] However, since in a classical MD simulation the charges of the atomic sites of the molecules are not updated during the run, such a simulation does not take into account the

Received: April 4, 2012
Revised: June 12, 2012
Published: June 13, 2012

dx.doi.org/10.1021/jp3032034 | J. Phys. Chem. B 2012, 116, 8169−8181

molecular polarization changes, which in turn would affect the conformational changes of a given solute molecule in the solvent.[28−30]

The effect of the molecular polarization on the conformation of a solvated molecule and, subsequently, on its absorption processes in a solvent environment has not been widely studied and is presently not well-understood. In this respect, the performance of a quantum Car−Parrinello MD (CPMD) simulation,[31] which takes into account the temporal evolution of both the solute molecular conformation and polarization, would represent an opportunity to get insight on this interesting issue. The present study was carried out focusing on precisely that. A representative azoaromatic molecule, disperse orange 3 (DO3), was studied by employing classical or hybrid CP QM/MM MD simulations in order to clarify the effect of the molecular polarization changes on the conformational changes and the 1PA and 2PA processes of this class of molecules in dimethyl sulfoxide (DMSO) solvent.

DO3 is a push−pull substituted pseudostilbene azoaromatic compound. The characteristic structure of the azo group between the aromatic rings enables a transition between the π and π^* molecular orbitals. Thus, this class of molecules has a one-photon absorption band in the vis region similar to the one observed for stilbene-type molecules. Furthermore, each nitrogen atom of the azo group provides a valence electron pair without bonding (lone pair) forming an *n*-type molecular orbital. These *n*-electrons can undergo transitions to the π^* orbital and, depending on the molecular symmetry, give rise to an absorption band in the vis region, which is not observed for stilbene-type molecules since they do not have lone pairs. The charge distribution of the $n \rightarrow \pi^*$ and $\pi \rightarrow \pi^*$ transitions are fundamentally different. The $n \rightarrow \pi^*$ transition involves the electron lone pairs of the azo group (−N═N−) and presents a weak charge-transfer character. However, the $\pi \rightarrow \pi^*$ transition can be of delocalized charge-transfer character, which can be further enhanced by the addition of charge donor and acceptor groups at the ends of the molecule. These two transitions, the lowest energy ones, are usually spectrally separated but can still overlap depending on the molecular symmetry.

The ordering of the two lowest energy excited states of pseudostilbene azoaromatic compounds can be altered due to their interaction with the solvent environment.[6,8,16,32] The ordering is strongly dependent on the strength of their donor and acceptor groups and in which solvent they are solvated.[16] Because of the low intensity related to the $n \rightarrow \pi^*$ transition, its experimental identification is not an easy task. Moreover, if these two lowest energy transitions are close in energy and since the transition accessing the $\pi \rightarrow \pi^*$ state is intense, the spectral band related to the $n \rightarrow \pi^*$ transition is often hidden. Such features make DO3 an interesting candidate for the present study.

The molecular conformation of DO3 in DMSO was monitored considering the changes of the main dihedral angles of its trans isomer during the simulations. Using a sequential procedure, calculations of spectroscopic parameters were a posteriori performed based on statistically uncorrelated configurations of the solute−solvent system.[33] In order to account for the solvent effects on the 1PA and 2PA of DO3 in a realistic way, a recently developed methodology, named the discrete polarizable embedding (PE) scheme,[34] was employed in the property hybrid QM/MM calculations. This methodology considers the conformational and polarization changes of the solute and the dynamical average of the solute−solvent system interaction, while still adopting a granular representation of the polarization and electrostatic interactions with the classically described solvent molecules (MM region). Defining a self-consistent reaction field procedure between the QM and MM regions of the total system, the mutual polarization between the solute and solvent molecules is reproduced by the PE scheme. The importance of using charge and polarizability decomposed interactions with the MM molecules has been demonstrated in some recent studies.[35,36]

In this study, the QM region is defined by the solute molecule. The PE calculations employed the response function formalism within the density functional theory (DFT) framework to describe the absorption processes. Because of the push−pull structure of DO3, its electronic transitions may contain a significant charge-transfer component. Therefore, in an effort to analyze the role of such a charge transfer process, the PE calculations were performed using the B3LYP[37,38] and CAM-B3LYP[39] functionals. Finally, the results obtained employing the uncorrelated configurations extracted from the hybrid CP QM/MM MD simulations were compared with the results recently reported in the literature for the 1PA and 2PA of dimethylamino nitro stilbene (DANS) in DMSO.[40]

2. METHODOLOGY

2.1. Dynamics. Two classical MD simulations were performed under normal conditions of temperature and pressure (T = 300 K; P = 1 atm). In the first simulation (simulation 1), the DO3 molecule was kept rigid (in the optimized geometry), and the solvent molecules were flexible. In the second simulation (simulation 2), both solute and solvent molecules were flexible. The simulated system is composed of 1 solute (DO3) molecule and 1280 solvent (DMSO) molecules in an orthorhombic box with a size of approximately 53.4, 54.8, and 51.4 Å. The intermolecular potential was defined by a Lennard-Jones (LJ) potential with the addition of the Coulombic (C) potential. The intermolecular interaction parameters provided by the General AMBER Force Field (GAFF),[41] which is implemented in the Amber 8 program,[42] were adopted to describe the LJ potential of both the solute and solvent molecules. The initial molecular conformation of the solute and solvent molecules were obtained from the geometry optimization at the B3LYP/6-311++G(d,p) level where the solvent effect on geometry was included through the IEF-PCM method[43] assuming the DMSO solvent. This B3LYP-PCM calculation provides a virtually planar conformation for DO3 in DMSO. One important aspect to consider prior to the classical MD simulations is the electronic polarization of DO3 and DMSO due to the solvent medium. To accomplish this polarization, the atomic charges of the Coulomb part of the potential of DO3 and DMSO were obtained using the electrostatic CHELPG mapping[44] at the level of B3LYP/aug-cc-pVTZ using the IEF-PCM solvent model and the optimized geometry of the solute and solvent molecules. All these DFT-PCM calculations were performed using the Gaussian03 package.[45]

The classical MD simulations were performed adopting the NPT ensemble and using the GROMACS program.[46,47] The total time of the MD run (with 1 fs time step) was 5 ns, and a total of 5×10^6 configurations were collected. After computing the energy autocorrelation function of these configurations,[33] 150 statistically uncorrelated configurations were adopted to perform the a posteriori PE response function calculations. The results of the PE calculations performed using the config-

dx.doi.org/10.1021/jp3032034 | J. Phys. Chem. B 2012, 116, 8169−8181

urations provided by these two classical MD simulations were compared in order to analyze the effect of the solute molecular conformational changes on its 1PA and 2PA processes.

A real solute−solvent system will also have contributions from mutual solute−solvent polarization, and there are reports that solvent-induced molecular conformational changes significantly contribute to the solute optical and magnetic properties. So, we carried out a third type, a hybrid Car−Parrinello (CP) QM/MM MD simulation (simulation 3), that can account for the effect of solute polarization by the solvent environment. In this simulation, only the DO3 molecule was described using a quantum mechanics approach (QM region), while the solvent molecules were described using classical force fields (MM region). The simulated system was composed of 1 solute molecule and 1280 solvent molecules in an orthorhombic box with dimensions of approximately 53.6, 54.9, and 51.5 Å. Since it is computationally expensive to equilibrate the whole solute−solvent system in the NPT ensemble, the initial, pre-equilibrated, structure for the hybrid CP QM/MM simulation was obtained from a classical MD simulation. The QM/MM Hamiltonian describes the coupling between the QM and MM regions and includes short-range repulsion, long-range attraction and electrostatic interactions between them.[44] In this work, the electronic wave function is expanded in a plane wave basis set with a cutoff energy of 80 Ry. The time step adopted to integrate the Hamiltonian equation of motion in this simulation was 5 au and the fictitious electronic mass used was 600 amu. The hybrid CP QM/MM MD simulation was performed using the CPMD/GROMOS software.[48−50] It starts with a quenching run which relaxes the initial structure to a Born−Oppenheimer surface of the QM/MM system. Subsequently, a temperature scaling run was performed to bring the system temperature to 300 K. The equilibration run was performed in NVT ensemble with the system connected to a Nose thermostat. The total time scale for the production simulation was about 15 ps.

2.2. QM/MM Response Calculations. To account for the solvent effects on the 1PA and 2PA of DO3, the recently developed PE scheme[34] was employed in the spectroscopic QM/MM calculations performed in this study. The use of a permanent charge distribution for the solvent molecules in the conventional nonpolarizable QM/MM methodologies considers only the polarization of the solute molecule due to the solvent environment, while the polarization effect in the opposite direction, i.e., the polarization of the solvent molecules due to the solute molecule is neglected. Usually, the solvent polarization is explicitly included in the conventional nonpolarizable QM/MM methodologies through the use of enhanced charges for its atomic sites. As in conventional QM/MM, the PE approach models the effects from an environment on a central core subsystem by including the effects directly in the density/wave function of the core system. However, in contrast to conventional QM/MM, the PE method is based on the use of a polarizable embedding potential. Thus, each atomic site is assigned a quantum mechanically derived multipole moment expansion to model the electrostatic embedding potential and an anisotropic dipole−dipole polarizability tensor to account for many-body induction effects, thus, allowing mutual polarization between the chromophore and the environment. In the present study, the MM multipole expansion is terminated at the charge level. The ground state electronic density of the chromophore is optimized while taking into account the explicit electrostatic interactions and polarization effects from the solvent environment in a fully self-consistent manner. The atomic charges used for DMSO in the present PE calculations were obtained through an electrostatic CHELPG mapping[44] calculation at the B3LYP/aug-cc-pVTZ level with the solvent molecule in gas-phase, and the distributed polarizabilities were obtained using the LoProp approach[51] at the B3LYP/aug-cc-pVTZ level of theory.

In this study, the QM region is composed by the DO3 molecule, i.e., only the solute molecule is explicitly considered. The PE calculations were performed using a development version of the DALTON program[52] and employed the response function formalism within the DFT framework to describe the absorption processes. In the response function formalism, the 1PA process is described by the linear response function, while the 2PA process is described by the quadratic response function.[53] The energy of the electronic transitions are determined as the poles of the linear response function, while the oscillator strengths of the 1PA transitions and the probabilities of the 2PA transitions are given by the first residues of the linear and quadratic response functions, respectively. The calculations were performed using either the B3LYP[37,38] or the CAM-B3LYP[39] functionals and the Turbomole-TZVP basis set[54] as implemented in the DALTON program.[52] Since DO3 is a push−pull molecule, the present study used two functionals to investigate the importance of properly describing the charge-transfer process present in the two-lowest energy electronic transitions of DO3 in solution. Moreover, the choice of using the CAM-B3LYP functional and the Turbomole-TZVP basis set in this study allowed to compare the results obtained for DO3 with results previously reported for the 1PA and 2PA of DANS in DMSO.[40] DANS and DO3 are push−pull aromatic molecules and distinguish by the nature of the π- electronic bridge in the middle of these systems and the strength of their electron donor groups.[9,11]

2.3. Two-Photon Absorption Cross-Sections. The 1PA and 2PA processes of DO3 in DMSO were here studied in a slightly different way. In the case of the 1PA process, this study tried qualitatively to explain the role of the solvent effects on the linear absorption spectrum of the chromophore along the vis region. For this, the statistically converged values of the oscillator strength and energy of the one-photon transitions were determined through QM and PE calculations performed for the uncorrelated configurations sampled from the three simulations. The statistical distributions of the energy of the lowest energy transitions of DO3 were also analyzed and the width of the line shape function describing such distributions estimated. In the case of the 2PA process, the present study provided a quantitative description of the role of the solvent effects on the 2PA process of DO3 along the vis region. For this, the statistically converged values of the two-photon transition probabilities and energies were determined through QM and PE calculations performed for the uncorrelated configurations sampled from the simulations. Using the values of the line width of the transitions, the 2PA cross-section of the two lowest excited states of DO3 were then estimated.

The 2PA cross-section (σ_{gf}) for a transition to a given excited state can be obtained by dividing the transition rate from the ground to the excited state by the square of photon flux. In 2PA experiments using the Z-scan technique,[55] for example, the amount of absorption is measured by the dissipation of the incident light, which for a single-beam setup is twice the

dx.doi.org/10.1021/jp3032034 | J. Phys. Chem. B 2012, 116, 8169−8181

transition rate. In this case, the 2PA cross-section of the degenerate process is written as[13,56,57]

$$\sigma_{gf}(\omega) = \frac{4\pi^3 \alpha a_0^5}{c}(\hbar\omega)^2 g(2\omega)\langle\delta_{gf}\rangle \quad (1)$$

where α is the fine structure constant, a_0 is the Bohr radius, c is the speed of light, ω is the angular frequency of the incident light (half of the transition angular frequency), $g(2\omega)$ is the normalized line shape function of the nth excited state, and $\langle\delta_{gf}\rangle$ is the two-photon transition probability for the transition from the ground state (g) to the nth final (f) excited state.

From a microscopic point of view, the central molecular quantity describing the two-photon absorption of a molecule in gas-phase is the two-photon transition matrix element. For a single beam experiment, and therefore a degenerate 2PA process, the two-photon transition matrix element is defined as[13,56,57]

$$S_{\alpha\beta}^{gf} = \frac{1}{\hbar}\sum_k \left[\frac{\langle g|\hat{e}\vec{\mu}_\alpha|k\rangle\langle k|\hat{e}\vec{\mu}_\beta|f\rangle}{\omega_{gk}-\omega} + \frac{\langle g|\hat{e}\vec{\mu}_\beta|k\rangle\langle k|\hat{e}\vec{\mu}_\alpha|f\rangle}{\omega_{gk}-\omega}\right] \quad (2)$$

where the subscripts α and β represent the Cartesian coordinates and g, k, and f refer to the ground, intermediate, and final electronic states, respectivelly. $\vec{\mu}_\alpha$ is the α-Cartesian component of the electric dipole moment operator, $\hat{e}$ is the unit vector describing the laser beam polarization. ω_{gk} is the angular frequency of the electronic transition from ground to an intermediate excited state, and ω is the angular frequency of each photon absorbed in the 2PA process, being $\omega = \omega_{gf}/2$, where ω_{gf} is the angular frequency of the electronic transition from the ground to the final excited state. The degenerate two-photon transition probability of a given transition for a molecule in a liquid environment (isotropic medium) is given by the orientational average of the two-photon matrix element. Using a linearly polarized laser beam, the two-photon transition probability is given by[58,59]

$$\langle\delta_{gf}\rangle = \frac{1}{30}\sum_{\alpha,\beta}\left[2S_{\alpha\alpha}^{gf}(S_{\beta\beta}^{gf})^* + 4S_{\alpha\beta}^{gf}(S_{\alpha\beta}^{gf})^*\right] \quad (3)$$

In this study, the two-photon transition matrix element is evaluated using expressions based on the response theoretical method. In this way, such molecular property is related to a first residue of the quadratic response function, and the explicit summation in eq 2 is avoided.

The line shape of the excited states is frequently represented by a well-known function; however, in the present work, we aim at avoiding the use of a predefined function. Considering the two-photon resonant condition, $\omega = \omega_{gf}/2$, and assuming a Lorentzian line shape function for the excited states, the 2PA cross-section is given by

$$\sigma_{gf}(\omega) = \frac{4\pi^3 \alpha a_0^5}{c}\frac{(\hbar\omega)^2}{\pi(\Gamma_f/2)}\langle\delta_{gf}\rangle \quad (4)$$

where Γ_f is the damping constant describing the full-width at half-maximum of the line shape function. As discussed by Ohta and co-workers,[56] the correct formula for the 2PA cross-section measured through a single-beam 2PA experiment differs from the Birge's equation,[60,61] derived for the case of a double-beam degenerate 2PA experiment, by a factor of 2. The correct formula for the two-photon matrix element in the case of a single-beam 2PA experiment is one-fourth of Birge's, and the correct formula for the 2PA cross-section is twice of Birge's, resulting in a factor of 2 in total. In the present work, we defined the two-photon matrix element (eq 2) as it is computed by the Dalton program;[52] the computed values are therefore twice the ones provided by the correct formula for a single-beam 2PA experiment. To make up for this factor, a constant equal to 4, instead of 16 as used by Ohta and co-workers,[13,56] is used in our formula for the 2PA cross-section (eqs 1 and 4). Therefore, the formulas adopted in the present work are consistent with the ones used by Ohta and co-workers,[13,56] and our results are correct for the case of single-beam 2PA experiments where the amount of nonlinear absorption is measured by the dissipation of the incident light.

3. RESULTS AND DISCUSSION

3.1. Molecular Conformation. The molecular planarity is an important factor for the 1PA and 2PA processes. Change of planarity affects the delocalization of the π electrons along the conjugation pathway and thereby changes the energy levels of the excited states, the one-photon oscillator strengths, and the two-photon transition probabilities. In this way, the molecular conformation of a solute molecule in a solvent environment may play a key role for understanding its spectroscopic behavior.

The fluctuations of the dihedral angles defined by the atoms 10−9−8−7 (angle 1) and 3−2−7−8 (angle 2), as illustrated in Figure 1, are the main changes observed in the molecular

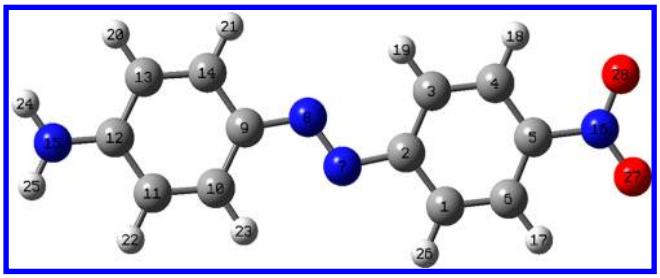

Figure 1. Molecular structure of disperse orange 3 (DO3) molecule. The white, gray, blue, and red spheres represent the hydrogen, carbon, nitrogen, and oxygen atoms, respectively.

conformation of the DO3 molecule during the classical and hybrid CP QM/MM MD simulations. The fluctuation of the dihedral angle defined by the azo group, i.e., by the atoms 2−7−8−9, was minimal (±3°) for all three simulations performed and therefore will not be further mentioned.

The values acquired by the dihedral angles 1 and 2 of DO3 during the classical MD simulation performed with both solute and solvent molecules flexible and the hybrid CP QM/MM MD simulation were plotted as a function of their occurrence. This graph is presented in Figure 2. As it can be noted, while for the classical MD simulation (Figure 2a), the average value of the dihedral angles 1 and 2 was zero, in the case of the hybrid CP QM/MM MD simulation, the average value of both dihedral angles was about 5°. The distribution of the values acquired by the angles 1 and 2 is very similar in the case of the classical MD simulation. However, for the hybrid CP QM/MM MD simulation, the distribution observed for the angle 2 is more spread than the one observed for the angle 1. Moreover, the distribution obtained for both dihedral angles is more spread in the hybrid CP QM/MM MD simulation than in the classical MD simulation and this is more evident for the angle 2.

dx.doi.org/10.1021/jp3032034 | J. Phys. Chem. B 2012, 116, 8169−8181

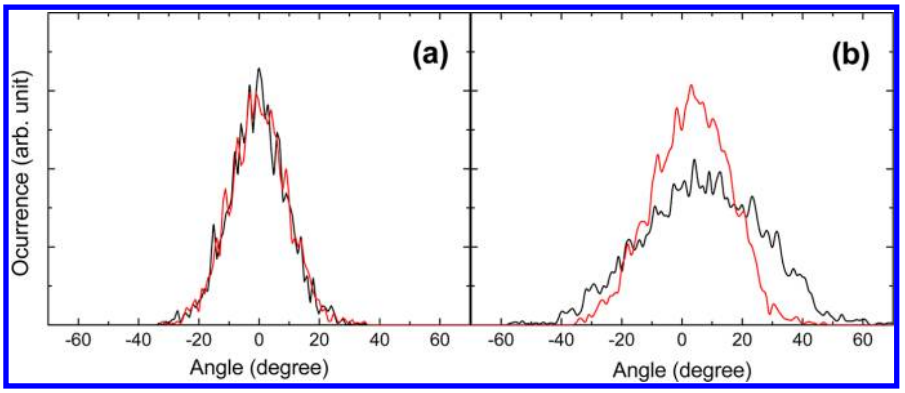

Figure 2. Fluctuation of the dihedral angle 1 (red line) and 2 (black line) during the classical MD (a) and hybrid CP QM/MM MD (b) simulations. The angles 1 and 2 are defined by the atoms 10−9−8−7 and 3−2−7−8, respectively (Figure 1).

Such differences are the result of the polarization changes on the conformational changes of DO3 along the simulation. Moreover, the distinct distributions obtained for the two dihedral angles in the case of the hybrid CP QM/MM MD simulation evidence that this simulation is sensitive to the charge character of the groups present at the ends of the aromatic rings of the azoaromatic molecule. This point seems to be overlooked by the classical MD simulation.

The equilibrium molecular conformation of azoaromatic compounds has been a subject of controversy for many years. The crystal structure of DO3 has not yet been reported. However, there seems to be little doubt that it is essentially planar taking into account the results of quantum chemical calculations reported for DO3 and related structures.[62−64] In the case of azobenzene, X-ray data[65] suggest a planar conformation in the crystalline phase, while gas-phase electron diffraction studies[66] suggest a nonplanar conformation with the phenyl rings twisted by 30° around the azo group plane (C−N=N−C). Both experimental techniques suggest that the dihedral angle defined by the azo group is virtually planar. A twisted molecular conformation is also found to be present in solution and has been supported by Raman measurements.[67]

MP2 calculations have indicated that DO3 and other pseudostilbene-type molecules have a twisted molecular conformation in gas-phase, and in addition, when solvent effects are taken into account using the PCM and adopting the DMSO solvent, the torsion angle between the aromatic rings of these molecules increases. However, DFT calculations in gas-phase provide planar molecular conformations for such molecules and slightly twisted conformations for calculations including solvent effects by using PCM.[64] These previously reported DFT and MP2 calculations also showed that the solvent effects are responsible for inducing (DFT) or increasing (MP2) the torsion between the aromatic rings of DO3 in DMSO. The torsion angle between the aromatic rings is the summation of the dihedral angles 1 and 2 defined in the present study. Therefore, the average value found for the torsion angle of DO3 in DMSO through the simulations 2 and 3 performed here are 0° and 10°, respectively. This value is close to the result of the DFT-PCM calculation reported (4°) for DO3 in DMSO,[64] however much smaller than the result of the MP2-PCM calculation (37°).[64]

3.2. One-Photon Absorption. The experimental linear absorption spectrum of DO3 in DMSO is basically composed of a broad band with a line width (full-width at half-maximum) of around 0.40 eV and centered at 485 nm (2.56 eV).[12] It is known that the $n \rightarrow \pi^*$ and $\pi \rightarrow \pi^*$ transitions of the azoaromatic molecules occur in the vis spectral region, and therefore, this band is ascribed to both transitions.[1,2] In Table 1,

Table 1. Energy (E_{gf} in eV) and Amplitude of the 1PA Transitions Acessing the Three Lowest Energy Excited States of DO3; the Amplitude of the 1PA Transitions Is Given by the Oscillator Strength (f_{gf})

			B3LYP		CAM-B3LYP	
simulation	system	trans	E_{gf}	f_{gf}	E_{gf}	f_{gf}
MD DO3 rigid	DO3	1	2.42	0.00	2.67	0.00
		2	2.89	0.92	3.29	1.12
		3	3.61	0.00	3.83	0.00
	DO3 + DMSO	1	2.36	0.25	2.71	0.03
		2	2.43	0.34	2.85	1.09
		3	3.36	0.04	3.95	0.00
MD DO3 flex	DO3	1	2.19	0.01	2.40	0.01
		2	2.93	0.56	3.53	0.61
		3	3.38	0.00	3.83	0.02
	DO3 + DMSO	1	2.09	0.10	2.42	0.03
		2	2.37	0.39	3.10	0.93
		3	3.08	0.01	3.83	0.00
hybrid CP QM/MM	DO3	1	2.33	0.07	2.58	0.04
		2	2.82	0.70	3.22	0.86
		3	3.29	0.00	3.55	0.01
	DO3 + DMSO	1	2.09	0.62	2.52	0.56
		2	2.35	0.18	2.84	0.52
		3	3.08	0.00	3.61	0,00

we present the results of the QM and PE linear response calculations for the three lowest energy transitions of DO3 in gas-phase and solvated in DMSO. Although the discussion presented here addresses only the two lowest energy transitions of the chromophore, the energy and intensity of the third lowest energy transition was also reported in Table 1 to clarify that, regardless of conformation changes and the solvent effects, such transition does not play a role in the description of the absorption of the chromophore in the vis region. These statistically converged values represent the average of the QM and PE calculations performed over 150 uncorrelated configurations sampled from each of the three simulations performed in this study. The result for DO3 rigid and in gas-phase is an exception; in this case, only a single QM linear response calculation was performed. First, all results obtained with DO3 in gas-phase will be compared, and we try to

dx.doi.org/10.1021/jp3032034 | J. Phys. Chem. B 2012, 116, 8169−8181

understand how the conformational changes during the simulations affect the 1PA process of DO3. It is important to clarify that the configurations with DO3 in gas-phase are, in fact, the snapshots taken from the classical and hybrid CP QM/MM MD simulations including DMSO, from where the solvent molecules were stripped for performing the a posteriori QM calculations. In the following, it will be presented and discussed how the solvent affects the 1PA process in the case of each simulation performed.

The B3LYP and CAM-B3LYP results for DO3 in gas-phase indicate that the oscillator strength of the one-photon transition to the first excited state is smaller than the oscillator strength of the one-photon transition to the second excited state. Comparing the results for simulations 1 (MD, DO3 rigid) and 2 (MD, DO3 flexible) one can realize that the conformational changes increased in about 1 order of magnitude the amplitude of the transition accessing the first excited state. However, such changes also diminish in about 25% of the amplitude of the one-photon transition accessing the second excited state. When the configurations sampled from simulation 3 (hybrid CP QM/MM MD) are used, the results in gas-phase indicate that the amplitude of the transition to the first excited state is even larger. For all three cases, the one-photon transition to the second excited state remains as the stronger transition.

The character of the two lowest energy transitions of DO3 was determined by analyzing the molecular orbitals involved in the excitations describing the electronic transitions. The two lowest energy transitions of DO3 are described by excitations involving basically four molecular orbitals. The molecular orbitals of DO3 were determined through QM and PE linear response calculations using the Turbomole-TZVP basis set and also employing the PCM for the planar and rigid conformation of DO3. The electron density distribution of these molecular orbitals does not apparently change either if QM or PE calculations are performed or if molecular conformations extracted from distinct simulations are adopted. The profile of the four molecular orbitals, obtained in DFT-PCM calculations adopting the planar and rigid conformation for DO3 is illustrated in Figure 3.

It is firmly settled that the first electronic transition of azobenzene is an $n \rightarrow \pi^*$ transition and the second one a $\pi \rightarrow \pi^*$ transition.[1,2] However, DO3 is a push−pull substituted pseudostilbene azoaromatic compound, and as already mentioned before, for this class of systems, the ordering of the two lowest energy transitions is strongly influenced by the solvent and the character of the charge groups present at the ends of its aromatic rings.[1,2,16] Therefore, the ordering of the two lowest energy excited states is still a subject of some controversy.

The coefficients of the excitations reported in Table 2 are the average values obtained from the calculations performed over the uncorrelated configurations sampled from each of the three simulations. On the basis of the coefficients and molecular orbitals involved in the excitations, the B3LYP and CAM-B3LYP results indicate that, in gas-phase, the first and lowest energy transition of DO3 is an $n \rightarrow \pi^*$ type and that the second transition is a $\pi \rightarrow \pi^*$ type. In both transitions, a substantial fraction of the electronic charge is transferred from an electron donor site of the molecule, $-NH_2$ or the azo group (lone pairs), to the region of the electron acceptor group ($-NO_2$); therefore, both are charge-transfer transitions. The conformational changes of DO3 (simulations 2 and 3) introduce a

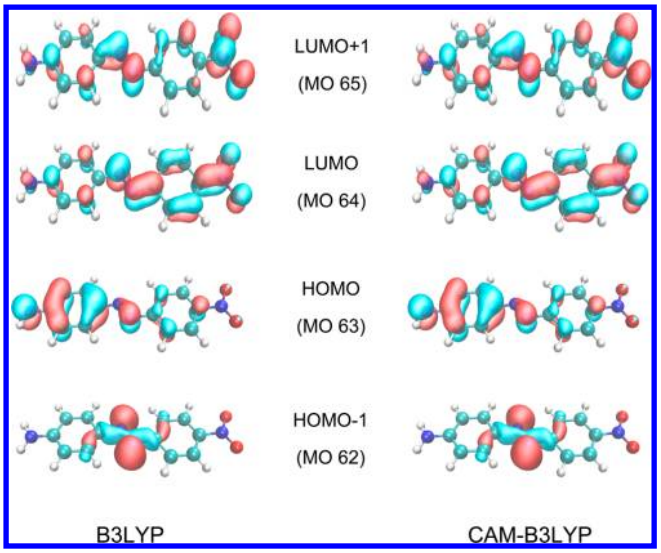

Figure 3. Molecular orbitals involved in the excitations describing the two lowest energy transitions of DO3 in DMSO. The molecular orbitals were obtained through DFT-PCM calculations using the Turbomole-TZVP basis set.

contribution of the π- (HOMO) and n- (HOMO − 1) type molecular orbitals to the first and second transitions, respectively; however, they basically do not change the character of the electronic transitions. Therefore, we conclude that the conformational changes and the strength of its charge groups are not enough to alter the excited state ordering of DO3 in comparison with the azobenzene molecule.

Concerning the effect of the solvent environment on the transitions, the results of the PE calculations performed over the configurations sampled from the classical MD simulations (simulation 1 and 2) and using the CAM-B3LYP functional indicate that, when DO3 is solvated, the $n \rightarrow \pi^*$ transition remains the lowest energy transition of the azoaromatic molecule. The amplitude of $n \rightarrow \pi^*$ and $\pi \rightarrow \pi^*$ transitions increase due to solvent effects, with the increase being particularly large for the $n \rightarrow \pi^*$ transition in the case of simulation 1. In addition, for both classical MD simulations, the one-photon transition to the second excited state, the $\pi \rightarrow \pi^*$ transition, remains as the stronger transition. However, the results obtained with the CAM-B3LYP functional for the configurations sampled from the hybrid CP QM/MM MD simulation (simulation 3) indicate that, when DO3 is solvated, the excitations involving both π- (HOMO) and n- (HOMO − 1) type molecular orbitals contribute substantially to the two electronic transitions. Because of this circumstance, it becomes more difficult to define the character of the two lowest energy transitions of DO3 when solvated in DMSO. Moreover, according to the CAM-B3LYP results, when DO3 is solvated, the amplitude of its two lowest energy transitions become rather similar.

The results obtained with the B3LYP functional indicate that the two lowest transitions of DO3 already lose their well-defined character in the case of the classical MD simulations. In the case of simulation 2, because of the considerable difference between the two main excitations, one can still assume the predominant character of the first and second electronic transitions as being $n \rightarrow \pi^*$ and $\pi \rightarrow \pi^*$ type, respectively. The B3LYP results indicate that the amplitudes of the two lowest energy transitions of DO3 become of the same order of

dx.doi.org/10.1021/jp3032034 | J. Phys. Chem. B 2012, 116, 8169−8181

Table 2. Excitations and Their Percentage Contributions to the Two Lowest Energy Transitions of DO3 in Gas-Phase and DMSO Solvent

		MD−DO3 rigid		MD−DO3 flex.		hybrid CP QM/MM MD	
system	trans	excit. (B3LYP)	excit. (CAM-B3LYP)	excit. (B3LYP)	excit. (CAM-B3LYP)	excit. (B3LYP)	excit. (CAM-B3LYP)
DO3	1	62 → 64, 92%	62 → 64, 79%	62 → 64, 54%	62 → 64, 63%	62 → 64, 63%	62 → 64, 63%
		62 → 65, 6%	62 → 65, 17%	62 → 65, 2%	62 → 65, 17%	62 → 65, 1%	62 → 65, 9%
		63 → 64, 0%	63 → 64, 0%	63 → 64, 14%	63 → 64, 0.3%	63 → 64, 17%	63 → 64, 2%
		63 → 65, 0%	63 → 65, 0%	63 → 65, 0%	63 → 65, 0%	63 → 65, 0%	63 → 65, 0%
	2	62 → 64, 0%	62 → 64, 0%	62 → 64, 16%	62 → 64, 1%	62 → 64, 16%	62 → 64, 3%
		62 → 65, 0%	62 → 65, 0%	62 → 65, 0%	62 → 65, 0%	62 → 65, 0%	62 → 65, 0%
		63 → 64, 100%	63 → 64, 92%	63 → 64, 65%	63 → 64, 44%	63 → 64, 70%	63 → 64, 65%
		63 → 65, 0%	63 → 65, 5%	63 → 65, 0%	63 → 65, 0.5%	63 → 65, 0%	63 → 65, 1%
DO3 + DMSO	1	62 → 64, 27%	62 → 64, 61%	62 → 64, 48%	62 → 64, 50%	62 → 64, 11%	62 → 64, 20%
		62 → 65, 2%	62 → 65, 22%	62 → 65, 1%	62 → 65, 16%	62 → 65, 0%	62 → 65, 3%
		63 → 64, 23%	63 → 64, 1%	63 → 64, 22%	63 → 64, 0.1%	63 → 64, 79%	63 → 64, 27%
		63 → 65, 0%	63 → 65, 0%	63 → 65, 0%	63 → 65, 0%	63 → 65, 0%	63 → 65, 0.2%
	2	62 → 64, 23%	62 → 64, 1%	62 → 64, 20%	62 → 64, 0.2%	62 → 64, 67%	62 → 64, 18%
		62 → 65, 2%	62 → 65, 0%	62 → 65, 0%	62 → 65, 0%	62 → 65, 2%	62 → 65, 4%
		63 → 64, 29%	63 → 64, 77%	63 → 64, 54%	63 → 64, 72%	63 → 64, 7%	63 → 64, 26%
		63 → 65, 0%	63 → 65, 6%	63 → 65, 0%	63 → 65, 7%	63 → 65, 0%	63 → 65, 0%

magnitude when the azoaromatic molecule is solvated. The results obtained for the configurations sampled from the hybrid CP QM/MM MD simulation (simulation 3) provides another description for the ordering of the two lowest energy excited states of DO3 solvated. In this case, on the basis of the percentage contribution of the MO excitations, one can identify the first lowest energy transition as the $\pi \rightarrow \pi^*$ transition and the second transition as the $n \rightarrow \pi^*$ transition. Therefore, the linear response calculations using B3LYP and CAM-B3LYP functionals provide similar descriptions for the two lowest energy transitions of DO3 in gas-phase for the three simulations performed in this study. When DO3 is solvated, however, the functionals provide distinct descriptions depending on the simulation considered. The results of the PE calculations using the B3LYP and CAM-B3LYP functionals only agree about the description of the two lowest energy transitions of DO3 in DMSO for the classical MD simulation performed with DO3 treated flexibly (simulation 2).

Because of the distinct descriptions provided by the B3LYP and CAM-B3LYP functionals and the prevailing controversy regarding the ordering of the two lowest energy transitions, in order to understand which results deserve greater confidence, the energy and solvatochromic shift of the transitions should also be carefully analyzed. In general, it is expected that an $n \rightarrow \pi^*$ transition experiences a small blueshift in polar solvents, while a $\pi \rightarrow \pi^*$ transition experiences a substantial redshift.[68] The results of the PE calculations using the CAM-B3LYP functional for the configurations sampled over the classical MD simulations, where the two lowest energy transitions have a well-defined character, are in agreement with this initial expectation concerning the solvatochromic shift of both transitions. The results obtained using the B3LYP functional for the classical MD simulations also indicate a substantial redshift for the second lowest energy transition, but in this case, the results indicate a small redshift for the first lowest energy transition. As already noted in these cases, the transitions lose their well-defined character, and this explains the unexpected solvatochromic shift of the first lowest energy transition. On the basis of the position of the broad band (2.56 eV) in the experimental 1PA spectrum of DO3 in DMSO solvent, one concludes that, in the case of the classical MD simulations, the PE calculations employing the CAM-B3LYP functional basically overestimate the energy of the two lowest energy transitions of DO3 in DMSO, the exception being the first transition for simulation 2, while the ones employing the B3LYP functional underestimate those energies.

In the case of the hybrid CP QM/MM MD simulation, the CAM-B3LYP results indicate that, for DO3 in gas-phase, the calculated energy of the first lowest energy transition (2.58 eV), an $n \rightarrow \pi^*$ transition, is close to the energy of the broad band in the experimental spectrum (2.56 eV). When DO3 is solvated, this transition exhibits a small redshift, unexpected for an $n \rightarrow \pi^*$ transition, and is therefore still in good agreement with the experimental data. Also, in this case, the unexpected direction of the solvatochromic shift of the first lowest energy transition is ascribed to the loss of its well-defined character. However, the calculated energy of the second transition of DO3 in gas-phase is much higher than the energy of the broad band in the experimental spectrum. Because of the solvent effects, the energy of this transition substantially diminishes but is still higher than the experimental value, and in addition, the well-defined character of this transition is also lost. In the case of the B3LYP functional, both transitions, which do not have a well-defined character even with DO3 in gas-phase, exhibit a substantial redshift when the solvent environment is taken into account. Therefore, the B3LYP calculations underestimate the energy of the two lowest energy transitions of DO3 in DMSO. Finally, it is also worthwhile comparing all the estimates of the energy of the second and stronger transition of DO3 in gas-phase present in this study with the experimental value (3.06 eV) for DO3 in cyclohexane solvent.[64] In this case, the CAM-B3LYP and B3LYP calculations in gas-phase again overestime and understimate, respectively, the energy of this transition. However, since it is expected that, in cyclohexane, the $\pi \rightarrow \pi^*$ transition already experience some redshift, we point out the performance of the CAM-B3LYP functional as the more accurate. Since the $\pi \rightarrow \pi^*$ transition of DO3 is a charge-transfer type, the more accurate description of the charge-transfer process by the CAM-B3LYP functional explains its more accurate results.

The use of the B3LYP functional for the transitions with charge-transfer character has to be done carefully. It has been

dx.doi.org/10.1021/jp3032034 | J. Phys. Chem. B 2012, 116, 8169−8181

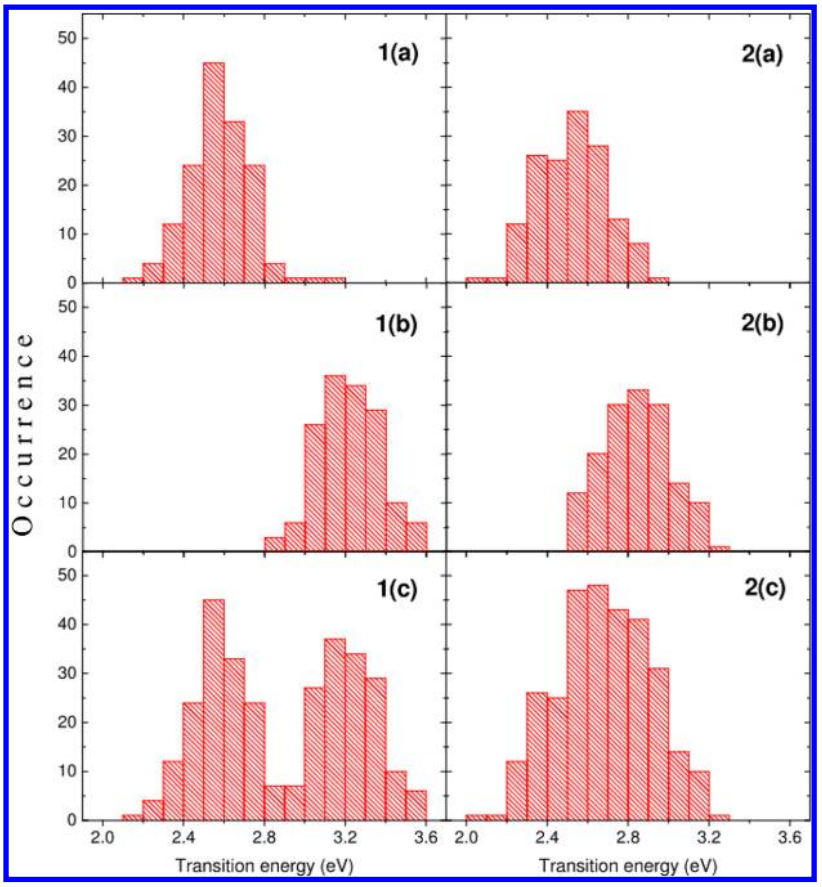

Figure 4. Histogram of the QM and PE calculations performed for the uncorrelated configurations sampled from the hybrid CP QM/MM MD simulation using the CAM-B3LYP functional. Case 1 (left column): DO3 in gas-phase. Case 2 (right column): DO3 in DMSO solvent. Occurrence of the first-lowest energy transition (a), the second-lowest energy transition (b), and of the both transitions together (c).

Table 3. Results of the 2PA Calculations for the Two Lowest Energy Excited States of DO3[a]

			B3LYP				CAM-B3LYP			
simulation	system	trans	E_{gf}	$\langle\delta_{gf}\rangle$	Γ_f	σ_{gf}	E_{gf}	$\langle\delta_{gf}\rangle$	Γ_f	σ_{gf}
MD DO3 rigid	DO3	1	2.42	4			2.67	2		
		2	2.89	31700			3.29	16500		
	DO3 + DMSO	1	2.36	107367	0.13	337.2	2.71	8235	0.10	44.3
		2	2.43	3009	0.24	5.4	2.85	56534	0.27	124.7
MD DO3 flex.	DO3	1	2.19	519	0.33	0.6	2.40	134	0.34	0.2
		2	2.93	42587	0.24	111.7	3.53	11979	0.26	42.1
	DO3 + DMSO	1	2.09	41047	0.39	33.7	2.42	1718	0.37	2.0
		2	2.37	114731	0.35	135.0	3.10	60733	0.30	142.5
hybrid CP QM/MM	DO3	1	2.34	1619	0.26	2.5	2.58	554	0.28	1.0
		2	2.82	30375	0.34	52.1	3.22	13658	0.36	28.8
	DO3 + DMSO	1	2.09	65274	0.44	47.5	2.52	41648	0.43	45.1
		2	2.35	36535	0.41	36.1	2.84	51323	0.40	75.9

[a] E_{gf} (in eV), $\langle\delta_{gf}\rangle$ (in a.u.), Γ_f (in eV), and σ_{gf} (in GM, Göppert−Mayer) are, respectively, the transition energy, the 2PA transition probability, the damping constant (describing a linewidth), and the 2PA cross-section of each excited state.

often shown that a B3LYP description for such transitions is associated with a significant error. The spatial overlap (Λ) computed for a given excitation has been used as a diagnostic parameter for its charge-transfer character.[69] Excitations associated with $\Lambda < 0.30$ have a larger charge-transfer character, and it is shown that the B3LYP functional exhibits larger error in describing such excitations. However, in the present case, the computed Λ values are between 0.4−0.6 for the two lowest energy transitions, which suggest that the usage of B3LYP functional is justified. The error in the excitation energies computed from CAMB3LYP functional is independent of this parameter (Λ).[69]

The two lowest energy transitions of DO3 are responsible for the single, broad, and no-structured band appearing in the vis region of the linear spectrum of DO3 in DMSO.[12] This broad band is centered at 2.56 eV (485 nm) and has a line width (full-width at half-maximum) of about 0.40 eV.[64] Therefore, either the two transitions are very close (or even overlapped) or the amplitude of one transition is much smaller/larger than the amplitude of the other one. The results of the QM calculations

dx.doi.org/10.1021/jp3032034 | J. Phys. Chem. B 2012, 116, 8169−8181

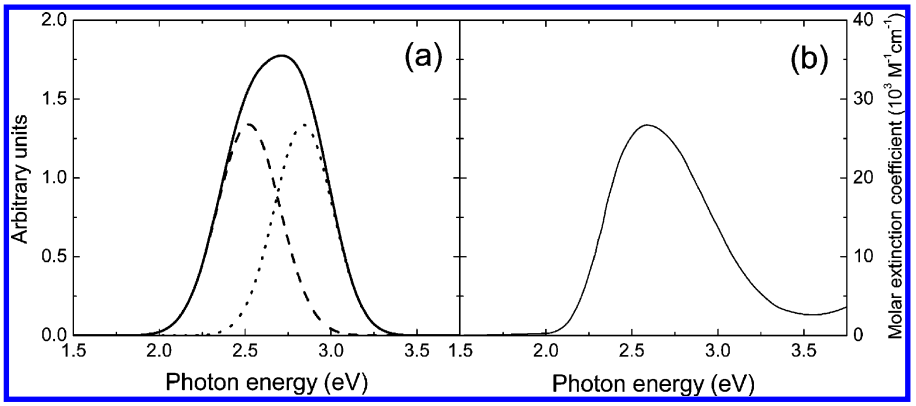

Figure 5. (a) Illustration of the final 1PA band of DO3 in DMSO solvent in the vis region simulated in this work. The dashed and dotted lines represent the 1PA band of the first and second excited states, respectively. (b) Experimental 1PA spectrum of DO3 in DMSO solvent (the experimental points were digitized).

performed for DO3 with the molecular conformations provided by simulations 2 and 3 indicate a difference between the average energy of the two lowest energy transitions of DO3 in gas-phase of about 0.45−1.10 eV. Therefore, even considering the statistical distributions of the energy of these transitions, the results of the QM calculations do not reproduce the single broad band of the linear spectrum of the chromophore.

Figure 4 presents the histogram of the QM and PE calculations performed for the uncorrelated configurations sampled from the hybrid CP QM/MM MD simulation using the CAM-B3LYP functional. The histogram shows how the solvent effects increase the overlapping of the bands of these two transitions. In the case of DO3 in gas-phase, besides the bands being more spaced apart, it should also be remembered that, in this case, the transitions have distinct amplitudes (Table 2). However, in the case of DO3 in DMSO, the transitions have similar amplitudes (Table 2), and the overlapping of the bands is clearly improved. The histogram, which takes into account the two lowest energy transitions together (Figure 4,2c), clearly evidence that the transitions form the broad and no-structured bands appearing at the vis region of the linear spectrum of DO3 in DMSO.

The result of the PE linear response calculations using the CAM-B3LYP functional and performed for the configurations extracted from the hybrid CP QM/MM MD simulation should be pointed out as the one in better agreement with the experimental 1PA spectrum of DO3 in DMSO solvent. In that case, the difference between the average energy of the two lowest energy transitions is 0.32 eV, and in addition, the transitions have similar amplitudes. To illustrate the broad 1PA band resulting from the partial overlap of the distributions of the two lowest energy transitions of DO3 in solution, we adopted a standard Gaussian line shape to mimic the distribution of each transition and assumed the line widths presented in Table 3. The approach employed to estimate the line widths is described in the next section. The final 1PA band obtained in this way has a peak in 2.70 eV (459 nm) and is presented in Figure 5. The experimental 1PA spectrum of DO3 in DMSO was extracted from ref 9 and is also presented in Figure 5 for direct comparisons. Moreover, the PE calculations using the B3LYP functional and performed for the configurations sampled from simulation 1 also seem to provide a reasonable result since the difference between the average energy of the two lowest energy transitions of DO3 in DMSO is only 0.07 eV in that case. However, it is important to remember that such simulation is the least advanced simulation performed in this work, and therefore, this result seems to be somewhat fortuitous.

Finally, as already mentioned, there exists a controversy regarding the ordering of the two lowest energy transitions of DO3 in solution. Moreover, it is commonly assumed that, in azocompounds, these transitions have a well-defined character, $\pi \rightarrow \pi^*$ and $n \rightarrow \pi^*$ type or vice versa.[1,2] Even some recent theoretical and experimental works have supported this assumption.[6,7,16,64] However, on the basis of the results of the PE calculations using CAM-B3LYP functional and performed over the configurations extracted from hybrid CP QM/MM MD simulation, our more sophisticated simulation, we preferentially conclude that, in DMSO, the two lowest energy transitions of DO3 lose their well-defined character. This is neither related to the conformation changes of the chromophore nor the strength of its charge groups but rather with the solvent-induced polarization. These findings contradict previous theoretical studies carried out employing a polarizable continuum model to describe the effect of solvent on the 1PA process of azocompounds in solution since these studies report that the electronic transitions of azocompounds in the vis region have a well-defined character.[6,7,16,64]

3.3. Two-Photon Absorption. The results of the QM and PE quadratic response calculations, using either the B3LYP or CAM-B3LYP functionals, for the configurations sampled from the three simulations performed are gathered in Table 3. These results indicate that, for DO3 in gas-phase, the 2PA transition probability (δ_{gf}) of the first excited state is small compared to the 2PA transition probability of the second excited state. The molecular conformational changes critically increase the probability of the 2PA transition to the first excited state, but it still remains much smaller than the probability of the 2PA transition to the second excited state in both simulations 2 and 3. In most cases, the 2PA transition probability of the first excited state is at least 2 orders of magnitude smaller. The results of the QM quadratic response calculations using the B3LYP and CAM-B3LYP functionals do not quanlitatively agree on the effect of the molecular conformational changes obtained throughout the classical MD simulation (simulation 2) on the 2PA transition probability of the second excited state of DO3 in gas-phase. However, the B3LYP and CAM-B3LYP results do agree about the effect of the molecular conformational changes obtained throughout the hybrid CP QM/MM MD simulation (simulation 3) on the 2PA transition

dx.doi.org/10.1021/jp3032034 | J. Phys. Chem. B 2012, 116, 8169−8181

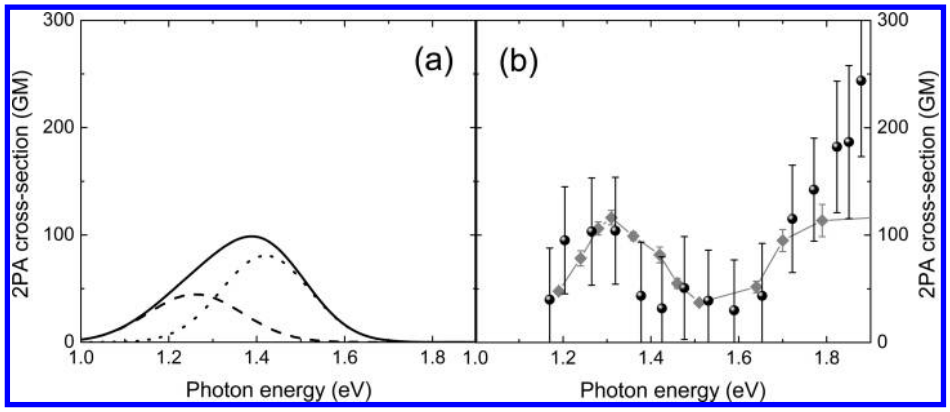

Figure 6. (a) Illustration of the final 2PA band of DO3 in DMSO solvent in the vis region simulated in this work. The dash and dot lines represent the 1PA band of the first and second excited states, respectively. (b) Experimental 2PA spectra of DO3 in DMSO solvent extracted from refs 9 (gray diamonds) and 12 (black balls). The experimental points were digitized.

probability of the second excited state compared with the chromophore in gas-phase. The probability of the 2PA transition to the second excited state is not critically affected by the conformational changes of DO3; the changes are smaller than 35% for both simulations 2 and 3.

When DO3 is solvated in DMSO, the results of the PE quadratic response calculations using the CAM-B3LYP functional indicate that the 2PA transition probability of the two lowest energy excited states increases. In the case of the classical MD simulations, the 2PA transition probability of the first excited state, despite being significantly enhanced, is still 1 order of magnitude smaller than the probability of the second excited state. However, when the PE calculations are performed over the configurations extracted from the hybrid CP QM/MM MD simulation, the 2PA probability of the two lowest energy states becomes comparable. The PE calculations using the B3LYP functional provide higher 2PA probabilities in comparison with the ones using the CAM-B3LYP functional. Except for the simulation 1, the B3LYP results also indicate that the solvent effects increase the 2PA probability of the two lowest energy excited states of DO3, and in the case of the simulation 3, it even makes the 2PA transition probability of the first excited state the larger one. Finally, taking into account the 2PA transition probability of both excited states, one can conclude that the molecular conformational changes of DO3 basically do not affect the total 2PA transition probability of the molecule along the vis region, while its interaction with the solvent environment increases it along this spectral region by about three to five times.

To obtain a quantitative description of the solvent effects on the two-photon absorption process of DO3 in DMSO, the 2PA cross-section (σ_{gf}) of the two lowest energy excited states were estimated. The strength of the approach adopted in the present study owes to the combination of the hybrid CP QM/MM MD simulation to sample the solute−solvent system and the PE response calculations, which account for solvent anisotropies and polarization interactions explicitly. This approach makes the calculations for the 2PA cross-sections now fully non-empirical since we do not need to assume a standard line shape function to estimate the spectral line width of the excited states to calculate the 2PA cross-sections (eq 4). The supposition of a standard value (usually set to 0.1 eV) for this crucial parameter has been a source of earlier discrepancy between the experimental and theoretical results. In this study, the spectral line width (Γ_f) is directly calculated from the linear response calculations as $\Gamma_f = 2(2 \ln 2)\nu_f^{1/2}$, where ν_f is the standard deviation of the excitation energies. This procedure is fully consistent for the PE calculations performed over the configurations from hybrid CP QM/MM MD simulation, where the contributions due to both homogeneous and inhomogeneous broadening of the absorbing state is taken into account.[40,70−72] In the case of the QM calculations performed for DO3 in gas-phase, the inhomogeneous contribution is neglected, and therefore, the value of the spectral line width of a given excited state is underestimated. The use of a classical MD simulation instead of a hybrid CP QM/MM MD simulation also compromises the accuracy in estimating the spectral line width. Therefore, although the above procedure is adopted to calculate the 2PA cross-section for all cases presented in Table 2 for the purpose of discussion, the results obtained for the case of the PE calculations performed over the configurations sampled from hybrid CP QM/MM MD simulation should be seen as the most consistent ones. The values estimated for the linewidths and the calculated for the 2PA cross-sections are presented in Table 3.

The values estimated for the linewidths from the PE calculations are larger than the ones estimated from the QM calculations, as expected. However, this effect, which could diminish the 2PA cross-section of the excited states, is not strong enough to compete with the effect of the solute polarization introduced by the PE scheme, which in turn enhances the 2PA transition probability of the two lowest energy excited states. Therefore, in all cases, the 2PA cross-section of DO3 in DMSO solvent is larger than in gas-phase, the exception being the cross-section of the second excited state for simulation 3 when the B3LYP functional is used. Through the PE calculations performed over the configurations sampled from the hybrid CP QM/MM MD simulation, the 2PA cross-sections of the first and second excited states were calculated to be 45.1 and 75.9 GM, respectively. The first and second excited states are separated in energy by around 0.32 eV, and since the linewidth of each of them is about 0.40 eV, the absorption band of these partially overlap. Therefore, in order to estimate the maximum value of the 2PA cross-section of DO3 along the vis region, one should consider the overlap of the two bands. In an effort to analyze the effect of such partial overlap of transitions, we now adopted a standard Gaussian line shape for each band, and assuming the parameters presented in Table 3, we obtained an illustration of the 2PA band of DO3 in DMSO solvent in the

dx.doi.org/10.1021/jp3032034 | J. Phys. Chem. B 2012, 116, 8169−8181

vis region. The final 2PA band obtained in this way is shown in Figure 6. The experimental 2PA spectrum of DO3 in DMSO is reported in refs 9 and 12. Those spectra are also shown here in Figure 6 for direct comparisons. It is worth remembering that the photon energy is equal to half of the transition energies shown in Table 3.

We finally note that a rigorous analysis of the shape of spectral lines in 1PA or 2PA can be only achieved by considering the full wave functions, electronic and vibrational, of the molecular system in ground and targeted excited states. In the force-field molecular dynamics technique, the sampling over low frequency normal mode is accounted for through a time evolution of molecular structure over the dihedral angle potential energy surface. In the hybrid CP QM/MM molecular dynamics, which follows the time evolution of a system at finite temperature, these low frequency modes are sampled explicitly. By treating nuclear motion in the molecule in a classical way via MD simulations, we certainly sample the evolution of electronic transition dipole moments and energies over the obtained MD trajectory and get so the dynamical contribution to the inhomogeneous broadening in the 2PA cross-section formula (in principle, also including zero-point motion). However, final state Franck−Condon factors are not explicitly accounted for. Such factors enter as a general broadening of the 2PA band but will, in principle, not enter the line shape function in the 2PA cross-section formula if one considers each electro-vibrational state individually.

The simulated 2PA band (Figure 6a) is centered around 1.38 eV (900 nm), and its peak value is about 98 GM. The energy of this point of maximum is about 0.10 eV higher than the energy of the peak of the experimental 2PA spectra in the vis region (Figure 6b). However, the peak value is in good agreement with the experimental data shown in Figure 6b, where the maximum 2PA cross-section in the vis region is reported to be about 100−120 GM.[9,12] The maximum value obtained here for the 2PA cross-section of DO3 in DMSO in the vis region is slightly larger than half of the 2PA cross-section recently calculated for DANS in DMSO solvent (149 GM) using the same scheme adopted in the present study.[40] This is in good agreement with the experimental work reported by Antonov and co-workers[9] for these two molecules. On the basis of a systematic study, Antonov and co-workers concluded that the difference between the 2PA cross-sections of these molecules in the vis region is not related to the nature of the π-electronic bridge in the middle of these systems but rather to the distinct strength of their electron donor groups. In the case of DANS, the nonlinear absorption amplitude in the vis region is ascribed to a single excited state. Finally, a detailed comparison between theoretical and experimental 2PA cross-sections calls for a careful consideration of how the experiments are performed since, in general, the extracted coherent 2PA cross-section is a mixture of pure 2PA plus one-photon excited state absorption, which tend to be very dependent on the characteristics of the laser pulse, especially the pulse length; see ref 73 for an earlier in-depth analysis of this issue.

4. SUMMARY AND CONCLUSIONS

In the present work, we have made an in-depth study of one- and two-photon absorption (1PA and 2PA, respectively) of Disperse Orange 3 (DO3), which shows conformational flexibility, embedded in dimethyl sulfoxide (DMSO) solvent. In this work, two classical and one hybrid Car−Parrinello (CP) QM/MM molecular dynamics (MD) simulations have been performed to describe the solvation of DO3 in DMSO. In the first classical MD simulation (simulation 1), the DO3 molecule was kept rigid and the solvent molecules were flexible, while in the second one (simulation 2) both solute and solvent molecules were flexible. A hybrid CP QM/MM molecular simulation (simulation 3), where only DO3 was described using a quantum mechanics approach, was also performed. This way, we pinpointed the importance of handling the effect of the conformational changes on the properties and of considering in detail how the solvent alters these conformations and how to perform proper dynamical sampling of those. The absorption spectrum of DO3 in the vis region is ascribed to its two lowest energy transitions, both charge-transfer type. Because of that, the response calculations were performed using the B3LYP and CAM-B3LYP functionals in order to analyze the importance of adopting an appropriate description of the charge-transfer process to study the 1PA and 2PA processes of the DO3 in DMSO.

The results of QM calculations performed for DO3 in gas-phase showed that the solvent-induced conformational changes increase the 1PA and 2PA intensities of the lowest energy transition of the chromophore and decrease the 1PA and 2PA intensities of its second lowest energy transition, which still remains the strongest one- and two-photon transition in the vis region. These results also showed that solvent-induced molecular conformational changes (simulations 2 and 3) do not alter the ordering and the well-defined character of the two lowest energy transitions of DO3. For all simulations, the first and second lowest energy transitions of DO3 in gas-phase are defined as $n \rightarrow \pi^*$ and $\pi \rightarrow \pi^*$ transitions, respectively. Moreover, except for the energy of the transitions, which are underestimated and overestimated by the B3LYP and CAM-B3LYP functionals, respectively, the functionals reasonably provide fairly similar descriptions for the 1PA and 2PA processes of DO3 when the chromophore is in gas-phase.

The results of the polarizable embedding (PE) calculations showed that, in DMSO, the 1PA and 2PA intensities of the two lowest energy transitions of DO3 increase. When performed over the configurations provided by classical MD simulations (simulations 1 and 2), the results of the PE calculations using both functionals showed that the second lowest energy transition remains as the strongest one- and two-photon transition of DO3 in the vis region after its solvation. The results also showed that, depending on the functional choice, the character of the lowest energy transition is affected by solvent effects. When the PE calculations are performed over the configurations provided by the hybrid CP QM/MM MD simulation (simulation 3), our more sophisticated simulation, the results provided by the B3LYP and CAM-B3LYP functionals indicate that the lowest energy transition become the stronger 1PA transition but disagree about which is the stronger 2PA transition and the role of the n-type and π-type molecular orbitals in these two transitions. To understand which of these results deserve greater confidence, the energy and the solvatochromic shift of the transitions were also carefully analyzed.

The solvent effects reduce the difference between the average energy of the two transitions and promote a partial overlap between the statistical distributions of their energies for all three simulations. Therefore, in most cases, the PE calculations reproduce the single and broad 1PA band of the linear spectrum of DO3 in the vis region. Taking the simple average of the energy of the two lowest energy transitions provided by

dx.doi.org/10.1021/jp3032034 | J. Phys. Chem. B 2012, 116, 8169−8181

the PE calculations performed over the configurations extracted from simulation 3, we realize that the CAM-B3LYP functional provides an average value (2.68 eV) in better agreement with the experimental value (2.56 eV, central wavelength of the broad 1PA band) than the B3LYP functional (2.22 eV). Therefore, we preferentially point out the performance of the CAM-B3LYP functional as the more accurate one and justify this based on the charge-transfer component acting in the two lowest energy transitions. Moreover, the results of the PE calculations were used to estimate the width of the line shape function of the two lowest energy excited states of DO3 in DMSO and allow us to obtain an empirical free prediction of their 2PA cross-sections. In the case of simulation 3, taking into account the additive effect promoted by the partial overlap of the bands of the excited states, this nonempirical prediction provided a maximum 2PA cross-section in good agreement with the experimental data available for DO3 in DMSO.

On the basis of the results of the CAM-B3LYP calculations performed over the configurations extracted from simulation 3, we conclude that, when DO3 is solvated in DMSO, its two lowest energy transitions do not have a well-defined character, as usually assumed, and both significantly contribute to its linear and nonlinear absorption in the vis region. Taking into account the 2PA of the two lowest energy transitions of DO3, we conclude that the solvation increases its nonlinear absorption in the vis region by about three times. In the case of the 1PA process, also taking into account the two lowest energy transitions, we conclude that the linear absorption of DO3 along the vis region increases by less than 50% due to its solvation in DMSO.

This work confirms the effect of the solvent to act both through direct intermolecular interactions and indirectly through inducing changes in the molecular conformation of the chromophore and therefore in its electronic structure and so alter its properties. Considering the distinct results obtained for the three simulations performed, we conclude that the direct and indirect effects of the solvent need to be accounted for on an equal footing. Indeed, the properties, especially here the 2PA cross-section, can be used to monitor the quality of the dynamics if proper experimental comparison is available. For example, on the basis of the comparison between our theoretical results and the experimental data, we could clearly settle the need for dynamics at the level of hybrid CP QM/MM MD as it provided a much better description of the solvation effect on the properties studied in comparison with the classical MD simulation. Moreover, this article settles the combined effect of conformation and solvent on the line shape function and provides a quantitative modeling of the 2PA cross-section of a chromophore in solution.

AUTHOR INFORMATION

Corresponding Author

*E-mail: dlsilva.physics@gmail.com.

Notes

The authors declare no competing financial interest.

ACKNOWLEDGMENTS

This work was supported by a grant from the Swedish Infrastructure Committee (SNIC) for the project "Multiphysics Modeling of Molecular Materials," SNIC 023/07-18. J.K. thanks The Danish Councils for Independent Research (STENO and Sapere Aude programmes), the Lundbeck Foundation, and the Villum foundation for financial support. D.L.S. and S.C. also gratefully acknowledge the partial financial support from FAPESP (Fundação de Amparo à Pesquisa do Estado de São Paulo), CNPq (Conselho Nacional de Desenvolvimento Científico e Tecnológico), and CAPES (Coordenação de Aperfeiçoamento de Pessoal de Nível Superior). D.L.S. is also grateful to the friendly hospitality of the Department of Theoretical Chemistry and Biology of the Royal Institute of Technology during his stay, when most of this work was conducted.

REFERENCES

(1) Rau, H. *Angew. Chem., Int. Ed.* **1973**, *12*, 224.
(2) Rau, H. Azo compounds. In *Photochromism, Molecules and Systems*; Dürr, H., Bouas-Laurent, H., Eds.; Elsevier: Amsterdam, The Netherlands, 2003; p 165.
(3) *Nonlinear Optics of Organic Molecules and Polymers*, 1st ed.; CRC Press, Inc.: Boca Raton, FL, 1997.
(4) Bortolus, P.; Monti, S. *J. Phys. Chem.* **1979**, *83*, 648.
(5) Asano, T.; Okada, T. *J. Org. Chem.* **1984**, *49*, 4387.
(6) Poprawa-Smoluch, M.; Baggerman, J.; Zhang, H.; Maas, H. P. A.; De Cola, L.; Brouwer, A. M. *J. Phys. Chem. A* **2006**, *110*, 11926.
(7) Toro, C.; Thibert, A.; De Boni, L.; Masunov, A. E.; Hernandez, F. E. J. *Phys. Chem. B* **2008**, *112*, 929.
(8) *Photoreactive Organic Thin Films*; Academic Press: New York, 2002.
(9) Antonov, L.; Kamada, K.; Ohta, K.; Kamounah, F. S. *Phys. Chem. Chem. Phys.* **2003**, *5*, 1193.
(10) Bartkowiak, W.; Zalesny, R.; Leszczynski, J. *Chem. Phys.* **2003**, *287*, 103.
(11) Day, P. N.; Nguyen, K. A.; Pachter, R. *J. Phys. Chem. B* **2005**, *109*, 1803.
(12) De Boni, L.; Misoguti, L.; Zilio, S. C.; Mendonca, C. R. *ChemPhysChem* **2005**, *6*, 1121.
(13) Ohta, K.; Antonov, L.; Yamada, S.; Kamada, K. *J. Chem. Phys.* **2007**, *127*, 084504.
(14) Day, P. N.; Nguyen, K. A.; Pachter, R. *J. Chem. Phys.* **2006**, *125*, 094103.
(15) Frediani, L.; Rinkevicius, Z.; Agren, H. *J. Chem. Phys.* **2005**, *122*, 244104.
(16) De Boni, L.; Toro, C.; Masunov, A. E.; Hernandez, F. E. *J. Phys. Chem. A* **2008**, *112*, 3886.
(17) Bredas, J. L.; Adant, C.; Tackx, P.; Persoons, A.; Pierce, B. M. *Chem. Rev.* **1994**, *94*, 243.
(18) Albota, M.; Beljonne, D.; Bredas, J. L.; Ehrlich, J. E.; Fu, J. Y.; Heikal, A. A.; Hess, S. E.; Kogej, T.; Levin, M. D.; Marder, S. R.; McCord-Maughon, D.; Perry, J. W.; Rockel, H.; Rumi, M.; Subramaniam, C.; Webb, W. W.; Wu, X. L.; Xu, C. *Science* **1998**, *281*, 1653.
(19) Wang, C. K.; Macak, P.; Luo, Y.; Agren, H. *J. Chem. Phys.* **2001**, *114*, 9813.
(20) Fu, J.; Padilha, L. A.; Hagan, D. J.; Van Stryland, E. W.; Przhonska, O. V.; Bondar, M. V.; Slominsky, Y. L.; Kachkovski, A. D. *J. Opt. Soc. Am. B* **2007**, *24*, 56.
(21) Terenziani, F.; Katan, C.; Badaeva, E.; Tretiak, S.; Blanchard-Desce, M. *Adv. Mater.* **2008**, *20*, 4641.
(22) De Boni, L.; Piovesan, E.; Misoguti, L.; Zilio, S. C.; Mendonca, C. R. *J. Phys. Chem. A* **2007**, *111*, 6222.
(23) Zhao, K.; Tu, Y. Q.; Luo, Y. *J. Phys. Chem. B* **2009**, *113*, 10271.
(24) De Boni, L.; Toro, C.; Zilio, S. C.; Mendonca, C. R.; Hernandez, F. E. *Chem. Phys. Lett.* **2010**, *487*, 226.
(25) Zhao, K.; Liu, P. W.; Wang, C. K.; Luo, Y. *J. Phys. Chem. B* **2010**, *114*, 10814.
(26) Pati, S. K.; Marks, T. J.; Ratner, M. A. *J. Am. Chem. Soc.* **2001**, *123*, 7287.
(27) Zalesny, R.; Bartkowiak, W.; Styrcz, S.; Leszczynski, J. *J. Phys. Chem. A* **2002**, *106*, 4032.

(28) Murugan, N. A.; Hugosson, H. W.; Agren, H. *J. Phys. Chem. B* **2008**, *112*, 14673.
(29) Murugan, N. A.; Kongsted, J.; Rinkevicius, Z.; Agren, H. *Proc. Natl. Acad. Sci. U.S.A.* **2010**, *107*, 16453.
(30) Oliveira, L. B. A.; Fonseca, T. L.; Coutinho, K.; Canuto, S. *Chem. Phys. Lett.* **2011**, *514*, 251.
(31) Car, R.; Parrinello, M. *Phys. Rev. Lett.* **1985**, *55*, 2471.
(32) Crecca, C. R.; Roitberg, A. E. *J. Phys. Chem. A* **2006**, *110*, 8188.
(33) Coutinho, K.; Canuto, S.; Zerner, M. C. *J. Chem. Phys.* **2000**, *112*, 9874.
(34) Nielsen, C. B.; Christiansen, O.; Mikkelsen, K. V.; Kongsted, J. *J. Chem. Phys.* **2007**, *126*, 154112.
(35) Olsen, J. M.; Aidas, K.; Mikkelsen, K. V.; Kongsted, J. *J. Chem. Theory Comput.* **2009**, *6*, 249.
(36) Olsen, J. M.; Aidas, K.; Kongsted, J. *J. Chem. Theory Comput.* **2010**, *6*, 3721.
(37) Lee, C. T.; Yang, W. T.; Parr, R. G. *Phys. Rev. B* **1988**, *37*, 785.
(38) Becke, A. D. *J. Chem. Phys.* **1993**, *98*, 5648.
(39) Yanai, T.; Tew, D. P.; Handy, N. C. *Chem. Phys. Lett.* **2004**, *393*, 51.
(40) Murugan, N. A.; Kongsted, J.; Rinkevicius, Z.; Aidas, K.; Mikkelsen, K. V.; Agren, H. *Phys. Chem. Chem. Phys.* **2011**, *13*, 12506.
(41) Wang, J. M.; Wolf, R. M.; Caldwell, J. W.; Kollman, P. A.; Case, D. A. *J. Comput. Chem.* **2004**, *25*, 1157.
(42) Case, D. A.; et al. *AMBER 8*; University of California: San Francisco, CA, 2004.
(43) Tomasi, J.; Mennucci, B.; Cammi, R. *Chem. Rev.* **2005**, *105*, 2999.
(44) Breneman, C. M.; Wiberg, K. B. *J. Comput. Chem.* **1990**, *11*, 361.
(45) Frisch, M. J.; Trucks, G. W.; Schlegel, H. B.; Scuseria, G. E.; Robb, M. A.; Cheeseman, J. R.; Montgomery, J. A., Jr.; Vreven, T.; Kudin, K. N.; Burant, J. C.; Millam, J. M.; Iyengar, S. S.; Tomasi, J.; Barone, V.; Mennucci, B.; Cossi, M.; Scalmani, G.; Rega, N.; Petersson, G. A.; Nakatsuji, H.; Hada, M.; Ehara, M.; Toyota, K.; Fukuda, R.; Hasegawa, J.; Ishida, M.; Nakajima, T.; Honda, Y.; Kitao, O.; Nakai, H.; Klene, M.; Li, X.; Knox, J. E.; Hratchian, H. P.; Cross, J. B.; Bakken, V.; Adamo, C.; Jaramillo, J.; Gomperts, R.; Stratmann, R. E.; Yazyev, O.; Austin, A. J.; Cammi, R.; Pomelli, C.; Ochterski, J. W.; Ayala, P. Y.; Morokuma, K.; Voth, G. A.; Salvador, P.; Dannenberg, J. J.; Zakrzewski, V. G.; Dapprich, S.; Daniels, A. D.; Strain, M. C.; Farkas, O.; Malick, D. K.; Rabuck, A. D.; Raghavachari, K.; Foresman, J. B.; Ortiz, J. V.; Cui, Q.; Baboul, A. G.; Clifford, S.; Cioslowski, J.; Stefanov, B. B.; Liu, G.; Liashenko, A.; Piskorz, P.; Komaromi, I.; Martin, R. L.; Fox, D. J.; Keith, T.; Al-Laham, M. A.; Peng, C. Y.; Nanayakkara, A.; Challacombe, M.; Gill, P. M. W.; Johnson, B.; Chen, W.; Wong, M. W.; Gonzalez, C.; Pople, J. A. *Gaussian 03*, revision D.01; Gaussian, Inc.: Wallingford, CT, 2003.
(46) Berendsen, H. J. C.; van der Spoel, D.; van Drunen, R. *Comput. Phys. Commun.* **1995**, *91*, 43.
(47) van der Spoel, D.; Lindahl, E.; Hess, B.; Groenhof, G.; Mark, A. E.; Berendsen, H. J. C. *J. Comput. Chem.* **2005**, *26*, 1701.
(48) Laio, A.; VandeVondele, J.; Rothlisberger, U. *J. Chem. Phys.* **2002**, *116*, 6941.
(49) Laio, A.; Vande Vondele, J.; Rothlisberger, U. *J. Phys. Chem. B* **2002**, *106*, 7300.
(50) Hutter, J.; Parrinello, M.; Marx, D.; Focher, P.; Tuckerman, M.; Andreoni, W.; Curioni, A.; Fois, E.; Rothlisberger, U.; Giannozzi, P.; Deutsch, T.; Alavi, A.; Sebastiani, D.; Laio, A.; Vande Vondele, J.; Seitsonen, A.; Billeter, S. *Computer code CPMD*, 3.11 ed.; Copyright IBM Corp. and MPI-FKF: Stuttgart, Germany, 1990−2002.
(51) Gagliardi, L.; Lindh, R.; Karlstrom, G. *J. Chem. Phys.* **2004**, *121*, 4494.
(52) DALTON, a molecular electronic structure program, 2011; see http://www.daltonprogram.org.
(53) Salek, P.; Vahtras, O.; Guo, J. D.; Luo, Y.; Helgaker, T.; Agren, H. *Chem. Phys. Lett.* **2003**, *374*, 446.
(54) Schafer, A.; Huber, C.; Ahlrichs, R. *J. Chem. Phys.* **1994**, *100*, 5829.
(55) Sheik-Bahae, M.; Said, A. A.; Wei, T. H.; Hagan, D. J.; Van Stryland, E. W. *IEEE J. Quantum Electron.* **1990**, *26*, 760.
(56) Ohta, K.; Kamada, K. *J. Chem. Phys.* **2006**, *124*, 124303.
(57) Boyd, R. W. Multiphoton Absorption and Multiphoton Ionization. In *Nonlinear Optics*, 2nd ed.; Academic Press: London, U.K., 2003; p 521.
(58) Monson, P. R.; McClain, W. M. *J. Chem. Phys.* **1970**, *53*, 29.
(59) McClain, W. M. *J. Chem. Phys.* **1971**, *55*, 2789.
(60) Birge, R. R.; Bennett, J. A.; Pierce, B. M.; Thomas, T. M. *J. Am. Chem. Soc.* **1978**, *100*, 1533.
(61) Birge, R. R.; Pierce, B. M. *J. Chem. Phys.* **1979**, *70*, 165.
(62) Morley, J. O. *J. Chem. Soc., Perkin Trans. 2* **1995**, *4*, 731.
(63) Morley, J. O. *J. Mol. Struct.* **1995**, *340*, 45.
(64) Silva, D. L.; Krawczyk, P.; Bartkowiak, W.; Mendonca, C. R. *J. Chem. Phys.* **2009**, *131*, 244516.
(65) Bouwstra, J. A.; Schouten, A.; Kroon, J. *Acta Crystallogr., Sect. C: Cryst. Struct. Commun.* **1983**, *39*, 1121.
(66) Tsuji, T.; Takashima, H.; Takeuchi, H.; Egawa, T.; Konaka, S. *J. Phys. Chem. A* **2001**, *105*, 9347.
(67) Kellerer, B.; Brandmul, J.; Hacker, H. H. *Indian J. Pure Appl. Phys.* **1971**, *9*, 903.
(68) Canuto, S., Ed. Solvation Effects on Molecules and Biomolecules. In *Computational Methods and Applications*; Springer: New York, 2008.
(69) Peach, M. J. G.; Benfield, P.; Helgaker, T.; Tozer, D. J. *J. Chem. Phys.* **2008**, *128*, 044118.
(70) Shemetulskis, N. E.; Loring, R. F. *J. Chem. Phys.* **1991**, *95*, 4756.
(71) Matyushov, D. V.; Ladanyi, B. M. *J. Chem. Phys.* **1997**, *107*, 1375.
(72) Polyutov, S.; Minkov, I.; Gel'mukhanov, F.; Agren, H. *J. Phys. Chem. A* **2005**, *109*, 9507.
(73) Baev, A.; Salek, P.; Gel'mukhanov, F.; Ågren, H. *J. Phys. Chem. B* **2006**, *110*, 5379.